Fe_2O_3 Nanoparticle Structures Investigated by X-ray Absorption Near-Edge Structure, Surface Modifications, and Model Calculations

Lin X. Chen,*,† Tao Liu,† Marion C. Thurnauer,† Roseann Csencsits,‡ and Tijana Rajh*,†

Chemistry Division and Materials Science Division, Argonne National Laboratory, Argonne, Illinois 60439

Received: January 23, 2002; In Final Form: June 6, 2002

The structures of Fe_2O_3 nanoparticles with different sizes were investigated using Fe K-edge X-ray absorption near-edge structure (XANES) and the FEFF calculations, as well as surface modification with enediol ligands. The studies not only revealed the existence of under-coordinated Fe sites in the nanoparticles but also confirmed that these under-coordinated sites were located on the surface. Upon binding of enediol ligands, surface sites were restructured to octahedral sites. In particular, the nature of the surface defects and their correlation with the unique properties of the nanoparticles were discussed. Model calculations were conducted for Fe_mO_n ($m \geq 1$, $n \geq 4$) clusters of various sizes centered at Fe sites with octahedral (O_h), distorted octahedral (C_{3v}) and tetrahedral (T_d) coordination geometry using FEFF8.10 programs. The main features of the calculated spectra agree with the experimental results and were correlated to the density of states, the Fe coordination geometry, and the long-range order of the lattice.

I. Introduction

Nanoparticles (NP) of transition-metal oxides have generated vast interest in recent years because of their unique properties that are not present in bulk materials.[1,2] Since these unique functions are closely correlated to the surface and the overall lattice structure of nanoparticles, it is essential to characterize the details of these structures. X-ray absorption near-edge structure (XANES) is sensitive to local geometries and electronic structures of atoms that constitute the NP. Therefore, changes of the coordination geometry and the oxidation state upon decreasing the particle size and the interactions with molecules adsorbed on the NP surface can be extracted from XANES spectra.[3] Moreover, X-ray absorption fine structure (XAFS) is precise in determining the local structure that may reflect the lattice disorder in NP. However, these techniques indiscriminately record local structural information for all atoms of a particular kind in the entire NP without distinguishing the location of the atoms (on the surface or in the interior). Therefore, coupling the structural information from XANES with chemical methods for surface modification enables characterization of the location and the nature of the structural changes in NP.

Our previous studies that measured XANES and XAFS spectra as a function of the NP size revealed structural origins of enhanced catalytic activities for titanium dioxide (TiO_2) NP that were related to the surface lattice distortions.[4,5] We found that the distorted octahedral coordination geometry of Ti in the bulk anatase was changed to a penta-coordination geometry on the surface of the NP. Such surface defects were responsible for the enhanced bonding with strongly interacting surface modifiers which change the optical properties and catalytic activities of the NP.

In this study, we expand our investigation on the structure/function relationship to ferric oxide (Fe_2O_3) NP that, by their own right, have been intensively studied because of the applications in magnetic storage, gas sensing, and catalysis.[6−11] Most of the ferric oxides are semiconductors with a band gap of a few electronvolts, for example, 2.2 eV for haematite.[12] Similar to several other metal oxide NP, the band gap and thus the properties of ferric oxide can be tuned via the particle size and the chemical environment.[13] To reveal the structural origins responsible for the unique properties of the NP, we explored size-induced electronic and geometric structural changes in the NP from those of the bulk. Like Ti atoms in TiO_2, Fe atoms in Fe_2O_3 possess partially filled 3d bands that give rise to the characteristic preedge features in XANES spectra, which are sensitive to the metal coordination geometry.

To correlate XANES spectral features with structures of Fe_2O_3 NP, we have also carried out model calculations on XANES spectra and angular momentum projected density of states (*l*-DOS) for Fe−O clusters centered at Fe sites with different symmetries. The calculations were based on known structures of the bulk lattices using the one-electron multiple-scattering approaches implemented in FEFF 8.10 programs.[14] In addition, we compared experimental XANES spectra of NP of different particle sizes with and without chemical modification of the surface with enediol ligands. The advantage of this chemical approach, as demonstrated by our previous studies on TiO_2, is being able to clearly distinguish changes occurring on the surface from those in the interior of the NP.

II. Experimental Procedure

Sample Preparation. The seeds of colloidal Fe_2O_3 NP were prepared by thermal hydrodialysis of $FeCl_3$ in water.[15,16] Accordingly, 6.5-nm NP were prepared by dropwise addition of $FeCl_3$ into hot water, and the temperature and rate of component mixing of reactants were carefully controlled. 3-nm particles were prepared by rapid injection of 10 mL of $FeCl_3$ into 90 mL of boiling water. Following the $FeCl_3$ hydrolysis,

* To whom correspondence should be addressed. E-mail: lchen@anl.gov, rajh@anl.gov. Fax: (630)252-9289.
† Chemistry Division.
‡ Materials Science Division.

10.1021/jp025544x CCC: $22.00
Published on Web 07/31/2002

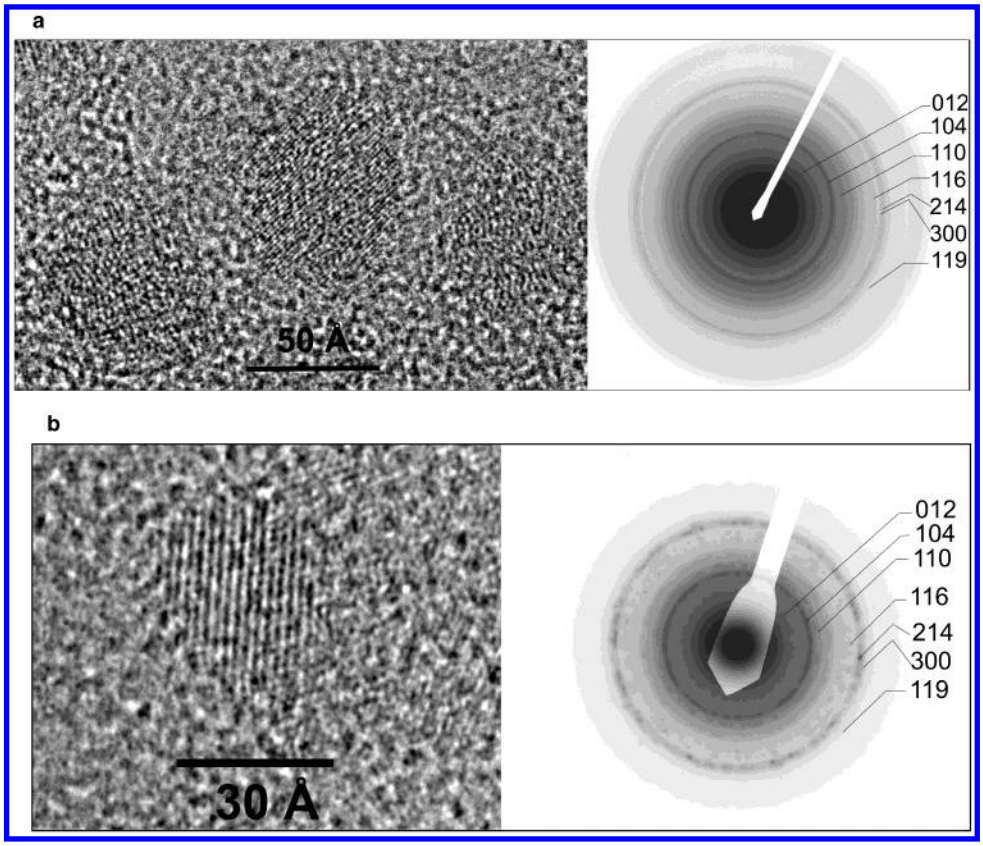

Figure 1. HRTEM images and the electron diffraction patterns of Fe_2O_3 nanoparticles with (a) 6.5-nm and (b) 3-nm diameters. The electron diffraction patterns of Fe_2O_3 NP were indexed by lattice parameters of the bulk α-Fe_2O_3.

the solution was incubated at 75 °C for 24 h and then was cooled to room temperature. The pH of the solution was between 1.2 and 1.8 depending on the $FeCl_3$ concentration. Analogous to the procedure developed for TiO_2 NP, the formation of seeds was followed by slow particle growth achieved by increasing the pH of the solution to pH 4 using dialysis at 4 °C.[17,18] A majority of the particles grew during dialysis because the solubility of iron oxide particles decreased from 0.01 M at pH 1.8 to 10^{-9} M at pH 4.[19] The concentration was controlled and determined using Inductively Coupled Plasma (ICP) spectrometry to be in the range of 0.02−0.1 M. The encapsulated NP were prepared by adding either ascorbic acid or dopamine into the NP solution. These surface modifiers were added in the amounts that correspond to the formation of a monolayer on the NP surface. Surface modified samples displayed an electron diffraction pattern of hematite with the same lattice parameters as unmodified samples.

Transmission Electron Microscope (TEM). Specimens for observation in the TEM were prepared by placing 1 or 2 drops of NP suspension onto holey carbon films supported on copper grids. These specimens were allowed to air-dry for at least 12 h. Specimens were imaged in a JEOL 100CXII TEM operating at 100 kV. High-resolution TEM (HRTEM) measurements were carried out on a JEOL 4000EXII TEM operating at 400 kV to record lattice images of individual particles.

X-ray Absorption Spectroscopy. XANES measurements were carried out at beamlines 12BM and 11ID-D of the Basic Energy Science Synchrotron Research Center, Advanced Photon Source at Argonne National Laboratory. Si 111 and 220 crystals were used respectively in the double-crystal monochromators of the two beamlines. The incident X-ray intensity was kept constant via a feedback system with 30% detuning to remove higher order harmonics. All spectra were collected at room temperature in the transmission mode. The monochromator energy was calibrated with the K-edge position of an Fe foil at 7.112 keV and was reproducible within 0.1 eV between the scans. NP samples were ground into fine powders and pressed into thin pellets. Each sample was sandwiched between two pieces of Kapton tape. α-Fe_2O_3 and γ-Fe_2O_3 (Aldrich) were chosen as bulk references. The data analysis was carried out with WinXAS.[20] Each spectrum was normalized by the edge jump defined by the preedge fit with a linear function and the postedge fit with a third polynomial.

III. Method of Calculation

XANES and DOS calculations were carried out using the FEFF8.10 program (University of Washington).[14] The first three neighboring atomic shells around the central absorbing Fe atom were constructed for the self-consistent field (SCF) potential calculations. XANES spectra were calculated using the Hedin−Lundqvist self-energy[21] with an energy dispersion of 1.0 eV to account for the core hole lifetime and the instrumental broadening effects. To produce the preedge peaks in XANES spectra that agreed with the experimental data, an energy adjustment of 2 eV was made for the Fermi level, E_F. The full multiple-scattering (FMS) calculations were used. The muffin-tin radii were automatically overlapped up to 1.15 to reduce discontinuities between adjacent regions of muffin-tin potentials. The Debye−Waller factors were set to zero because of their negligible influence on XANES spectra. Because XANES directly reflected the *l*-DOS of the final states following the selection rules for dipolar transitions, its specific features were related to electronic structures of the absorbing atoms.[14]

IV. Results and Discussion

Although the coordination geometry of the interior atoms in NP was largely believed to have the same lattice structure as

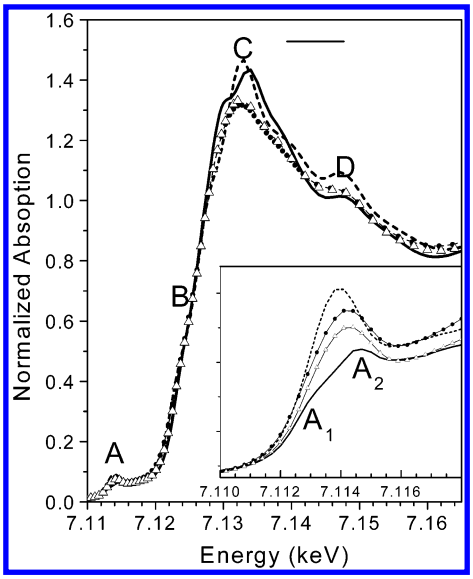

Figure 2. XANES spectra of NP, bulk α-Fe_2O_3 and γ-Fe_2O_3. Inset: the preedge region of the spectra. Spectral features described in the text are labeled accordingly.

the bulk, the coordination geometry of the surface atoms could substantially differ from that of the bulk, forming surface defect sites with energy levels in the mid-gap region. These changes at the surface could propagate further toward the NP core, causing interior lattice disorder. XANES spectra of NP were expected to reveal both surface and interior lattice disorder through the spectral features that directly reflected changes in the structural and electronic properties of NP from those of bulk metal oxides. The lower conduction bands of transition-metal oxides were mainly composed of transition-metal 3d orbitals, while the upper valence bands were mainly composed of oxygen p orbitals.[22] Because of crystal fields of different lattices, these 3d orbitals of the lower conduction bands were split into sub-bands that gained p-character by mixing with p-orbitals of the central metal atom or neighboring oxygen atoms. Absorption of X-rays that resulted from the transition of a 1s electron to these sub-bands exhibited near-edge features in metal oxide XANES spectra. Furthermore, preedge features in XANES spectra of transition-metal K-edge were attributed to (a) quadrupole transitions from 1s to 3d orbitals,[23] (b) dipole-allowed transitions due to the 3d−4p mixing of the metal, and (c) d−p mixing between the metal atom and ligands through bonding and multiple scatterings involving the same atoms with different scattering paths.[24] Therefore, the positions of the preedge peaks directly reflected the crystal field splitting of 3d orbital sub-bands, and intensities of the preedge features were sensitive to the local coordination geometry of the metal atom. Moreover, other XANES features originated from distant multiple scatterings could be used to probe lattice disorder in NP.

Structural Changes in Nanoparticles. HRTEM images and electron diffraction patterns of both 6.5- and 3-nm NP designated well-crystalline particles and mainly α-Fe_2O_3 rombohedral corundum lattice structure (Figure 1). Experimental XANES spectra of Fe_2O_3 NP with average diameters of 6.5- and 3-nm were depicted in Figure 2, along with those of bulk. Apparently, the intensity of the preedge peak for γ-Fe_2O_3 was significantly higher, and the position of the peak was 0.7 eV lower in energy than those for α-Fe_2O_3. Interestingly, preedge features for the NP were between those of α- and γ-Fe_2O_3 in terms of both intensity and the peak position, and the deviation from α-Fe_2O_3 was increasing with decreasing particle size (Figure 2 inset). Such differences can be attributed to differences of local

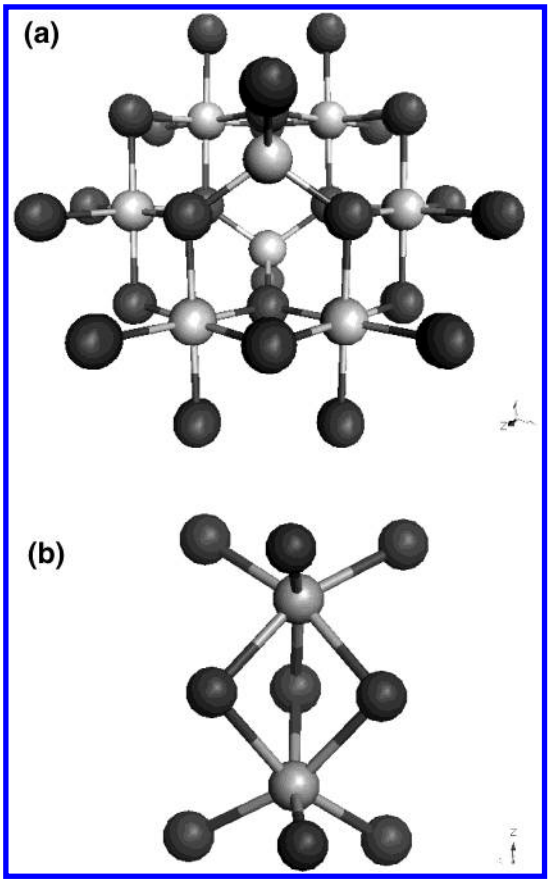

Figure 3. Fe sites in (a) maghemite, γ-Fe_2O_3, and (b) heamatite, α-Fe_2O_3. Light spheres are Fe atoms and dark spheres are O atoms.

symmetry of the Fe sites in these samples. The lattice structure of γ-Fe_2O_3 consisted of Fe sites with both O_h and T_d symmetries (Figure 3a) in a relative ratio of 1:0.6 and Fe−O bond lengths of 2.094 and 1.876 Å, respectively.[25] In contrast, α-Fe_2O_3 lattice only had distorted octahedral Fe sites with C_{3v} symmetry and two sets of three Fe−O bonds of 1.96 and 2.08 Å long, respectively (Figure 3b).[25]

To assign the spectral changes shown in Figure 1 to distortions of the Fe sites on the NP surface or NP interior, calculations were first carried out for Fe_mO_n ($m \geq 1$, $n \geq 4$) clusters centered at Fe sites with O_h, T_d, and C_{3v} symmetries, respectively, which served as models for correlating spectral features with structural origins.

Fe Sites with O_h Symmetry. On the basis of the octahedral Fe sites in bulk γ-Fe_2O_3 lattice structure, XANES spectra for Fe_mO_n clusters centered at an O_h Fe site were calculated (Figure 4a). Because of its centrosymmetry, the 4p−3d mixing in Fe atom was minimal, so the 1s to 3d transitions were mainly from quadrupole interactions.[26,27] Indeed, the preedge peak A was almost invisible in the FeO_6 cluster (Figure 4a). Because quadrupole interactions were not explicitly included in the FEFF calculation, the source for an extremely weak magnitude of peak A would have to come from mixing of the 3d orbitals of Fe with p orbitals of the neighboring atoms via higher order multiple-scattering paths. The preedge peak A in Figure 4a represented a situation where no dipole-allowed transition was present and could be used as a reference to separate contributions of dipole-allowed transitions from those of higher order multiple scatterings to the preedge features. Features C and D grew narrower and more intense and shifted to higher energies with the cluster size, indicating their origins of higher order distant multiple scatterings. Features C and D remained the same as

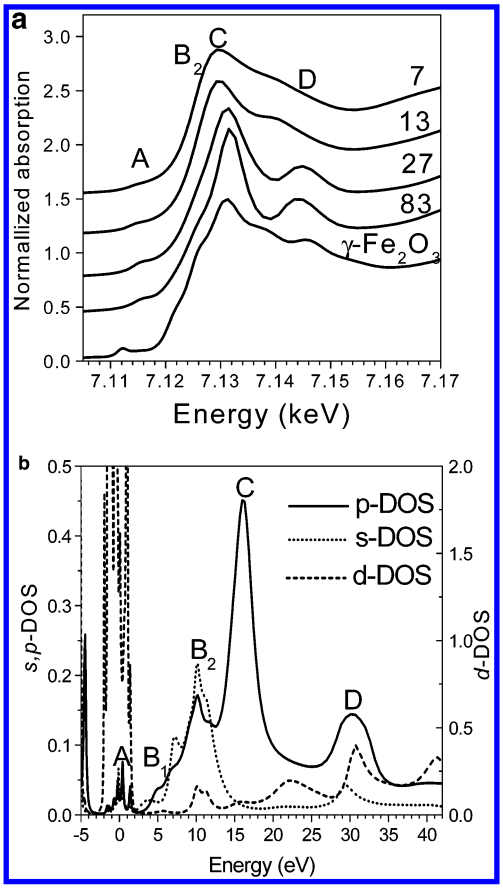

Figure 4. (a) Calculated Fe K-edge XANES spectra for Fe_mO_n clusters centered at an O_h Fe site based on γ-Fe_2O_3 structure. The numbers indicate total number of atoms in each cluster. The main features are labeled as A, B_1, B_2, C, and D. Experimental spectra are also included for comparison. (b) *l*-DOS for an 83-atom cluster centered at the O_h site. The main spectral features are labeled as A, B_1, B_2, C, and D, in accordance with those in (a). The energy zero indicates the Fermi level.

the central Fe was surrounded by three or more neighboring atom shells, suggesting an effective range of distant multiple scatterings, that is, 4 Å from the central Fe atom.

s-, p-, and d-DOS calculations for an 83-atom cluster with a 1s core hole were carried out (Figure 4b). Because of the selection rules for the electronic transitions, XANES features at the Fe K-edge were dominated by transitions from 1s to vacant p-component containing orbitals (Figure 4b), and thus largely coincided with the p-DOS. Peaks in the region A of p-DOS, corresponding to the preedge peak A in XANES spectra, were weak, consistent with a minimal mixing of 3d with p-component in O_h sites. Peaks B_2, C, and D in the p-DOS were related to a shoulder at 7.128 keV, the white light peak at 7.133 keV, and a peak at 7.146 keV in the γ-Fe_2O_3 spectrum (Figure 4a), respectively. Experimentally observed XANES features at 7.123 and 7.139 keV were missing in the calculated spectra. Because the s-, p-, and d-DOS all have a peak at B_2, the corresponding XANES feature could result from the transitions to the orbitals with 3d−4s−4p mixing. However, p-DOS dominated at C, so the corresponding white light peak was mainly from 1s to 4p transitions and multiple scatterings involving p-orbitals of both Fe and O. The calculation indicated that the white light peak C and peak D were mainly due to the contribution of the O_h sites.

Fe Sites with T_d Symmetry. XANES spectra for the Fe_mO_n clusters centered at an Fe site in T_d symmetry were calculated (Figure 5a) on the basis of the tetrahedral Fe sites in bulk γ-Fe_2O_3 lattice structure. Compared to the Fe sites in O_h

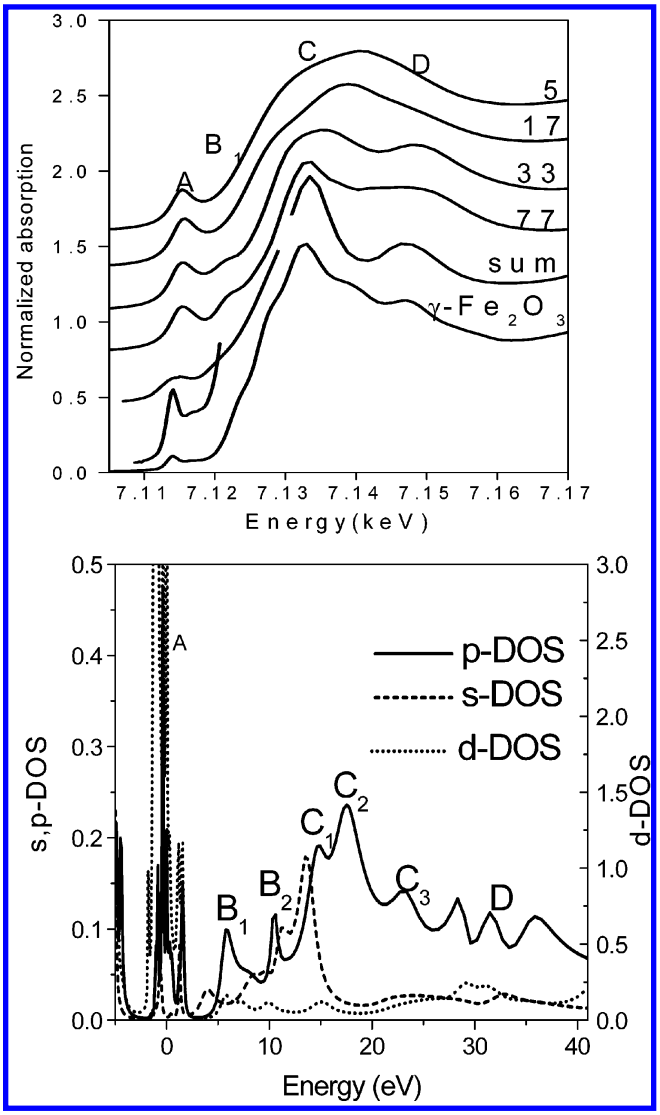

Figure 5. (a) Same as Figure 4 for clusters centered at a T_d Fe site based on γ-Fe_2O_3 structure; (b) *l*-DOS for a 77-atom cluster centered at the T_d site.

symmetry, the preedge peak A of FeO_4 (Figure 5a) was much more pronounced because of the noncentrosymmetric T_d crystal field that enabled dipole-allowed transitions. While preedge feature A was essentially independent of the cluster size because of its localized nature, features B_1 and D became more pronounced and peak C grew sharper because of their distant multiple-scattering origin. Compared to the O_h sites, peak C for the T_d sites was broader and weaker, confirming that the main contribution to the white light peak C in the γ-Fe_2O_3 spectrum was from the O_h sites. The features in region A of p-DOS (Figure 5b) had much higher amplitude than those for the O_h sites and coincided with d-DOS features, suggesting a p−d mixing as expected in noncentrosymmetric T_d sites. Since peak B_1 in the γ-Fe_2O_3 spectrum and the p-DOS were much more intense in the T_d site than in the O_h site, and they only appeared in larger clusters, it originated from the T_d sites with a lattice structure that facilitated higher order multiple scatterings. This assessment was supported by the fact that B_1 was experimentally observed only in crystalline materials but not in disordered Fe^{3+}-containing silicate glass.[25] Compared with Figure 4b, p-DOS above 15 eV of the Fermi level had a larger number of peaks with more dispersed energies and lower intensities, producing a "flatter" appearance in the spectrum above the transition edge. Hence, the overall calculated XANES

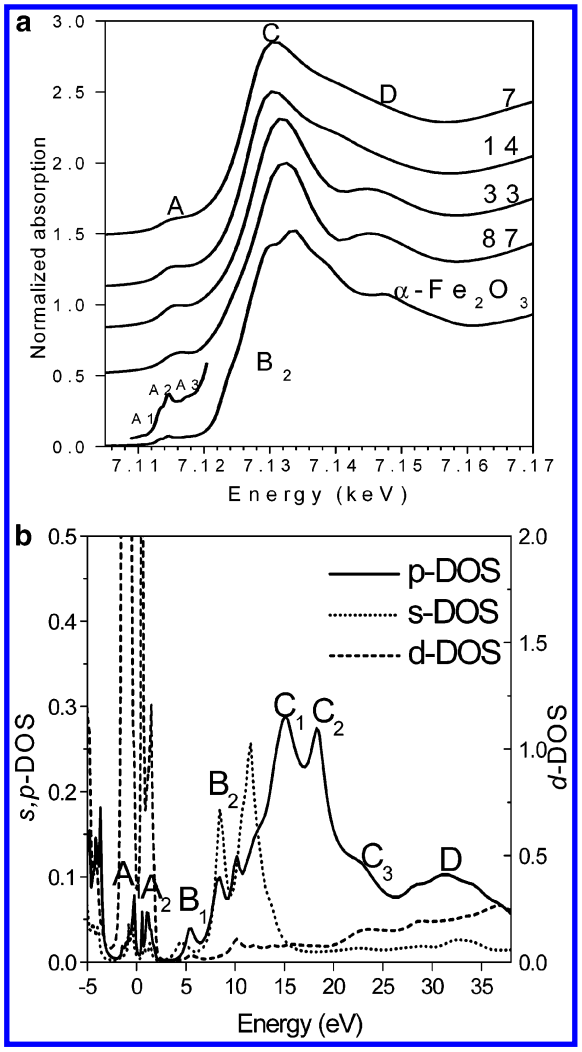

Figure 6. (a) Same as Figure 4 for clusters centered at a C_{3v} Fe site based on α-Fe_2O_3 structure. (b) *l*-DOS for an 87-atom cluster centered at the C_{3v} site.

spectrum for γ-Fe_2O_3 from the weighted average of the spectra for O_h and T_d sites (Figure 5a) can be explained by the DOS results showing that C and D are mainly from contributions of the O_h sites, while B_1 and B_2 were, respectively, from the T_d and O_h sites.

Fe Sites with C_{3v} Symmetry. Parallel calculations based on the distorted octaderal Fe sites in the bulk α-Fe_2O_3 lattice structure were carried out for Fe sites in C_{3v} symmetry (Figure 3b).[25] Although similar calculations were done by Wu et al.,[28] it was necessary to conduct consistent FEFF calculations for Fe sites with different geometries to achieve parallel comparison with experimental data.

The preedge peak A for the FeO_6 cluster in C_{3v} symmetry (Figure 6a) was more intense than that in O_h symmetry (Figure 4a) but weaker than that of the FeO_4 in T_d symmetry (Figure 5a), confirming its origin of the 3d−4p mixing in the Fe atom. Peak A was essentially unchanged in clusters with 14 or more atoms, suggesting its origin from the p−d mixing of the central Fe atom with the nearest two neighboring shells. Apparently, the fine preedge features A_1, A_2, and A_3 in the experimental spectrum (Figure 6) were not reproduced by the calculations. Such a discrepancy could be due to the 1-eV bandwidth used in the calculations, which produced a fine agreement with XANES spectra but less well-resolved preedge features. However, these fine features were seen in p-DOS (Figure 4b, 5b, and 6b) and qualitatively agreed to the extent of the p-component involvement in the 1s to 3d transitions.

Similarly, peaks C and D grew narrower and more intense and shifted to higher energies with the particle size. However, none of the calculated spectra reproduced the peak C splitting as in the experimental data, although such spitting was revealed in the p-DOS (C_1 and C_2 in Figure 5b). The absence of such splitting in calculated spectra was partially attributed to the spectral broadening because of the core hole lifetime and the instrumental broadening effect that was taken into account in the calculations. The other possible cause was neglecting nonspherical potential in directional Fe−O bonding in the FEFF calculations. A similar phenomenon was also seen in the calculations for transition-metal monoxides where it was attributed to the nonspherical corrections from directional metal-O bonds.[29]

On the basis of the above calculations that reproduced most of the XANES features in the experimental spectra, we identified the structural origins of the preedge and other main features in the XANES spectra. When a high spin ground-state Fe^{3+} [$(3d^5)$, $(t_{2g})^3(e_g)^2$] was surrounded by an O_h crystal field, 1s electron could be promoted to both t_{2g} and e_g sub-bands. This was supported by the previous assignment of the preedge peaks A_1, A_2, and A_3 to transitions from 1s to t_{2g}, e_g, and higher conduction sub-bands, respectively.[30] In contrast, a T_d crystal field generally split 3d orbitals into e and t_2 sub-bands,[31] which produced an intense preedge peak resulting from transitions from 1s to both sub-bands that overlapped because of an energy splitting that was smaller than the instrumental resolution.[25]

The experimentally obtained preedge features of the NP spectra were enhanced compared to those of α-Fe_2O_3 (Figure 2), suggesting that Fe sites in NP were further distorted from the C_{3v} octahedral Fe sites in α-Fe_2O_3 into under-coordinated T_d or square-pyramidal structure. However, according to the electron diffraction and HRTEM images (Figure 1b), the lattice structure of the NP was the same as that of α-Fe_2O_3 for both 6.5- and 3-nm particles. The discrepancy between XANES and TEM results could be interpreted by different emphasis of the techniques. The electron diffraction patterns were obtained by diffractions from the ordered core lattice and were disturbed very little from the surface truncation. Hence, surface layers with different lattice structures contributed very little to an electron diffraction pattern. Likewise, lattice fringes in the HRTEM images were obtained when the lattice layers in the NP were aligned, and the significant electron absorption occurred only when multiple layers were present. Hence, very little contribution from misaligned surface layers was responsible for shaping an observable image. Therefore, TEM techniques emphasized structures of majority atoms in the core of NP. In contrast, an XANES spectrum was a statistical average of all sites from the entire NP. When the surface lattice differed from that of the core, the XANES spectrum deviated from that of the bulk, and the deviation would be proportional to the number of surface sites. For this very reason, we investigated the surface structure of NP using very small particles where a significant fraction of metal atoms was present on the particle surface. Accordingly, the intensities of these preedge features were more intense for NP with 3-nm diameter than those with 6.5-nm diameter, which can be rationalized by the larger fraction of surface atoms and therefore more pronounced deviation from the bulk crystalline structure in the former than in the latter. Using the parameters for α-Fe_2O_3 lattice, fractions of surface Fe sites were estimated to be 24% and 52% for the NP with diameters of 6.5- and 3-nm, respectively.

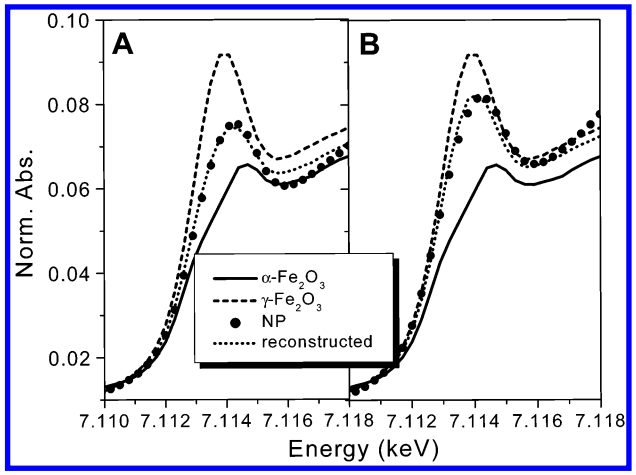

Figure 7. Preedge region of XANES spectra for NP with (A) 6.5-nm and (B) 3-nm diameters, along with those of bulk α-Fe_2O_3 and γ-Fe_2O_3. Dotted curves were reconstructed from sums of α-Fe_2O_3 and γ-Fe_2O_3 spectra with relative fractions corresponding to the ratios of the octahedral sites: the tetrahedral sites 83:17 in (A) for 6.5-nm NP and 73:27 in (B) for 3.0-nm NP. Dots were experimental data.

To quantitatively correlate the distortion of Fe sites in NP with the number of surface sites, we reconstructed the preedge features for the NP with 6.5- and 3-nm diameters from those of the octahedral and tetrahedral Fe sites obtained from the experimental spectra of the bulk Fe_2O_3 on the basis of the following approximations. (1) The surface defects could be treated as mostly T_d sites; (2) the preedge intensities for all octahedral sites, with O_h or C_{3v} symmetry, were the same; (3) the defects appeared on a single surface layer. The reconstructed preedge peaks of NP were obtained by mixing the spectra of γ- and α-Fe_2O_3 where the former had 63% O_h and 37% T_d sites and the latter had 100% octahedral sites. The ratio of the mix was chosen to match the preedge peak height from the experimental data. For the best fits between the reconstructed and experimental data, the fraction of the surface sites are 17 and 26% for NP with 6.5- and 3-nm diameters, respectively (Figure 7), which were lower than calculated surface fractions of 24 and 52% on the basis of the α-Fe_2O_3 lattice structure. Such a discrepancy suggested that some surface sites could have coordination symmetry that gave less intense preedge peak than T_d, such as pentacoordinated square-pyramid geometry, or that some of the surface sites retain octahedral geometry.

In addition to the above consideration, features C and D were less distinctive for NP than for the bulk, especially for the white light peak C, which was indicative of long-range disorder. As shown in the FEFF calculations, the intense peak C required at least three neighboring shells of atoms around an Fe site. Thus, any lattice inhomogeneity that could attenuate distant multiple scatterings would attenuate the white light peak C. Consequently, those attenuated spectral features in NP likely indicated lattice distortions in the second layer of Fe sites from the absorbing Fe sites.

Structural Changes in Nanoparticles upon Binding of Surface Modifiers. XANES spectra alone were not able to disclose uniquely whether the lattice disorder was localized on the NP surface or propagated throughout the entire NP. Coordination defects from the interior lattice distortion and local strains in the NP, as well as under-coordination of the surface sites, all led to the noncentrosymmetry of the Fe site and thus to the enhancement of preedge peak A. Although the fraction of the under-coordinated sites has been shown to increase with the fraction of surface sites, we need to demonstrate that these surface sites could be changed upon modification of the NP surface, and uniquely identify the location of the under-coordinated sites. Apparently, the preedge peaks A_1 and A_2 observed in bulk α-Fe_2O_3 merged into a single broad peak A in NP. A possible disorder in the nanoparticle lattice that produced diverse energy levels of 3d orbitals could be responsible for such a spectral broadening. Because of finite sizes of the NP, forces that were responsible for the long-range order in the bulk were disturbed. In addition, distortions of surface defects could penetrate a couple of atomic layers as seen on the surface of Fe_2O_3 thin films.[32] Meanwhile, the core of a NP may experience little or no effect from the surface distortion, and thus retain the bulk lattice structure.

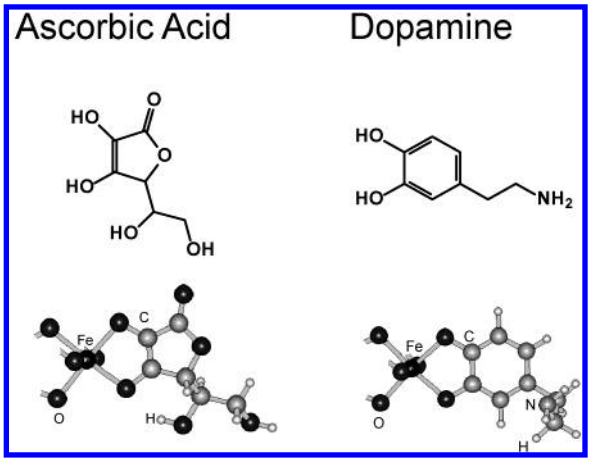

Figure 8. Structures of DA and AA as well as their proposed binding configurations with surface Fe sites in Fe_2O_3 nanoparticles.

One way to distinguish the surface defects from those of the interior was to selectively modify surface sites by binding enediol ligands to the surface Fe sites. Bidentate enediol ligands were chosen because of their ability to chelate Fe ions and to establish their favorable octahedral environment. Upon the binding, the coordination environment of surface Fe sites was altered, while the coordination of interior Fe sites remained unchanged.[4,5] The differences in XANES spectra of NP with and without the surface-binding ligands were used to identify spectral features that were due to the surface structural modification. This surface modification drastically altered band structures of metal oxides as well as their optical properties, suggesting strong couplings of the ligand to the nanoparticle surface.[33] Figure 8 depicted structures for two such enediol ligands, ascorbic acid (AA) and dopamine (DA), as well as their plausible bidentate binding configurations with the surface Fe sites of NP on the basis of our previous studies.[5,34] The magnitudes of preedge feature A in XANES spectra of both NP-DA and NP-AA were reduced from that of unmodified NP approaching that of α-Fe_2O_3 (Figure 9 inset), signaling a recovery of under-coordinated Fe surface sites back to a bulklike lattice structure with octahedral sites upon the chelation with bidentate enediol ligands. The recovery of the coordination number of Fe surface sites was also confirmed via XAFS data analysis where the coordination number of the nearest neighboring shell in surface modified samples was consistently higher than that of unmodified NP.[35] In addition, the white light peak C for surface modified NP became more pronounced compared to that of unmodified NP and was almost as intense as that of α-Fe_2O_3 (Figure 9), similar to that shown in calculated XANES spectra for large clusters with a longer range order (Figures 4b and 6b). This was consistent with the calculated results that peak C was mainly produced by octahedral Fe sites. Hence, the lower intensity of C in the unmodified NP compared to the bulk revealed fewer octahedral sites in NP because of surface

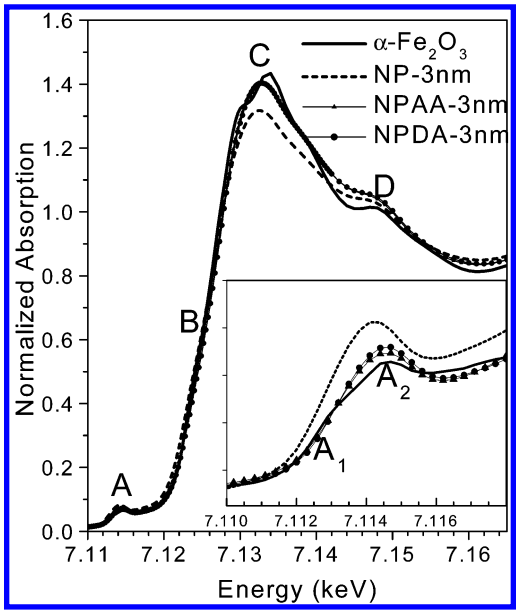

Figure 9. XANES spectra of NP, NP-DA, and NP-AA along with that of α-Fe_2O_3. Inset: the preedge region of all the spectra. Spectral features mentioned in the text are labeled accordingly.

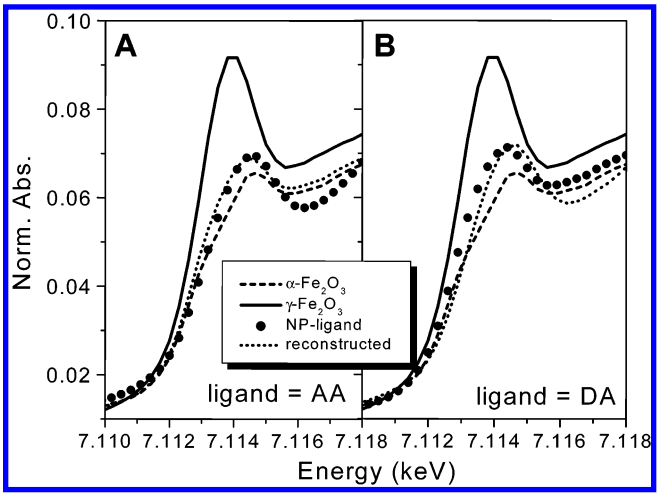

Figure 10. Preedge region of XANES spectra for 3-nm NP with and without the surface binding ligands, along with those of α- and γ-Fe_2O_3. Dotted curves were reconstructed from sums of the spectra of α-and γ-Fe_2O_3 with relative fractions corresponding to the ratios of the octahedral sites: the tetrahedral sites 92:8 in (A) for NP-AA and 88:11 in (B) for NP-DA. Comparing 8 and 11% of defect sites with 26% defect sites in unmodified NP, 70 and 58% recovery were estimated for NPAA and NP-DA, respectively. Dots were experimental data.

truncation, whereas the recovery of peak C upon the surface modification was strong evidence for an increase in the number of octahedral sites on the NP surface. Since the calculations show that peak C was not influenced by the atoms farther than 4 Å from the absorbing Fe atom, the structural changes mainly took place within this range. The higher intensity and the narrowing of peak C upon surface modification implied that the restructuring on the particle surface enhanced the homogeneity of the NP lattice by forming favorable octahedral surface Fe sites. This observation is in accord with the previous studies on surface modified TiO_2 NP where DA and AA bind surface Ti atoms via two adjacent hydroxyl groups chelating surface metal atoms (Figure 8).[5]

Although the preedge peak intensity recovered to near the level of the bulk upon binding with the ligands on the NP surface, the recovery was incomplete, and the fine spectral features A_1, A_2, and A_3 observed in bulk α-Fe_2O_3 did not reappear. The results suggested that the recovered octahedral sites could have distinctively different fine structures from the interior lattice, which bought upon a broader distribution in energies of the t_{2g} and e_g orbitals, and consequently smeared-out the fine preedge features. To estimate the fraction of the surface Fe sites that were recovered from the defect Fe sites on the surface upon surface modification, we reconstructed the preedge spectra of modified NP by mixing those of α- and γ-Fe_2O_3 as we did for the NP without modification in the last section with the same approximations. Although the absolute number of the defect sites could not be estimated by this reconstruction, the relative fraction of the recovery could be calculated. The reconstructed preedge spectra for NP-AA and NP-DA (Figure 10) suggested 70 and 58% recovery of the defect sites. Similar findings were obtained for binding enediol ligands on TiO_2 surfaces using Langmuir adsorption isotherm.[33] The high fractions of the recovery upon the binding of the surface modifiers, therefore, identified the surface sites as the main source of the defect sites in NP. The apparent less than perfect recovery of the defect sites could be attributed to incomplete binding of all surface sites because of the steric hindrance between ligands, the difference in the coordination environments and nearest neighbor distances of the recovered octahedral sites on the surface from those in the interior, and the exclusion of pentacoordinate sites in the calculation.

V. Summary

The Fe_2O_3 NP were identified to have the interior lattice structure of α-Fe_2O_3. Correlations between XANES spectral features and their structural origins were made through model FEFF calculations in terms of coordination geometries and electronic configurations of the Fe sites and were applied to the investigation of NP structures. The preedge peaks in K-edge XANES spectra became more pronounced as the Fe site increasingly deviated from the centrosymmetric O_h geometry because of the mixing between 3d orbitals with p-components from Fe itself or from O ligands. The main spectral features above the transition edges had mainly p-like character and were sensitive to the long-range order of the lattice. XANES and angular momentum projected DOS calculations for the Fe/O clusters centered at Fe sites with O_h, T_d, and C_{3v} geometries, respectively, achieved good agreement with experimental data of α-Fe_2O_3 and γ-Fe_2O_3 and demonstrated the effectiveness of using the one-electron multiple-scattering theory with a muffin-tin approximation.

Using the structure/spectrum correlation established from the calculations and the size-dependent preedge peak intensity in the NP XANES spectra, the nature of the surface defects of Fe_2O_3 NP was established as under-coordinated Fe sites with one or two O ligands missing from that of an octahedral coordination. The XANES spectra of NP with bound enediol groups of DA and AA confirmed that the majority of the structural changes took place on the surface sites that were responsible for the unique interfacial chemistry of the nanoparticles.

Acknowledgment. This work is supported by the Division of Chemical Sciences, Office of Basic Energy Sciences, U.S. Department of Energy, under contract W-31-109-Eng-38. TEM analysis was carried out in the Electron Microscopy Collaborative Research Center at Argonne National Laboratory. We would like to thank Professors J. J. Rehr and A. L. Ankudinov from the University of Washington for useful discussions on FEFF

calculations. The assistance from BESSRC-CAT personnel at Beamline 12BM and ID-11D, Advanced Photon Source, Argonne National Laboratory is greatly appreciated.

References and Notes

(1) Gleiter, H. *Adv. Mater. (Weinheim, Ger.)* **1992**, *4*, 474.
(2) Siegel, R. W. *Sci. Am.* **1996**, *275*, 74.
(3) Iwasawa, Y. *Ser. Synchrotron Radiat. Technol. Appl.* **1996**, *2*, 2.
(4) Chen, L. X.; Rajh, T.; Wang, Z.; Thurnauer, M. C. *J. Phys. Chem. B* **1997**, *101*, 10688.
(5) Rajh, T.; Nedeljkovic, J. M.; Chen, L. X.; Poluektov, O.; Thurnauer, M. C. *J. Phys. Chem. B* **1999**, *103*, 3515.
(6) Bein, T.; Tielen, M.; Jacobs, P. A. *Ber. Bunsen-Ges. Phys. Chem.* **1986**, *90*, 395.
(7) Zhang, L.; Papaefthymiou, G. C.; Ziolo, R. F.; Ying, J. Y. *Nanostruct. Mater.* **1997**, *9*, 185.
(8) Mayer, C. R.; Cabuil, V.; Lalot, T.; Thouvenot, R. *Angew. Chem., Int. Ed.* **1999**, *38*, 3672.
(9) Yu, B.; Zhu, C.; Gan, F. *Physica E (Amsterdam)* **2000**, *8*, 360.
(10) Horvath, D.; Toth, L.; Guczi, L. *Catal. Lett.* **2000**, *67*, 117.
(11) Dubois, E.; Perzynski, R.; Boue, F.; Cabuil, V. *Langmuir* **2000**, *16*, 5617.
(12) Zhang, Z.; Boxall, C.; Kelsall, G. H. *Colloids Surf., A* **1993**, *73*, 145.
(13) Alivisatos, A. P. *J. Phys. Chem.* **1996**, *100*, 13226.
(14) Ankudinov, A. L.; Ravel, B.; Rehr, J. J.; Conradson, S. D. *Phys. Rev. B: Condens. Matter* **1998**, *58*, 7565.
(15) Brusov, K. N.; Us'yarov, O. G. *Kolloidn. Zh.* **1988**, *50*, 627.
(16) Milonjic, S. K.; Vucic, N. B.; Vujosevic, S. I. *Sep. Sci. Technol.* **1996**, *31*, 1515.
(17) Rajh, T.; Tiede, D. M.; Thurnauer, M. C. *J. Non-Cryst. Solids* **1996**, *205*−*207*, 815.
(18) Rajh, T.; Saponjic, Z. V.; Micic, O. I. *Langmuir* **1992**, *8*, 1265.
(19) Baes, C. F., Jr.; Mesmer, R. E. *The Hydrolysis of Cations*; 1976.
(20) Ressler, T. *J. Synchrotron Radiat.* **1998**, *5*, 118.
(21) Hedin, L.; Lundqvist, S. *Solid State Phys.* **1969**, *23*, 1.
(22) Asahi, R.; Taga, Y.; Mannstadt, W.; Freeman, A. J. *Phys. Rev. B: Condens. Matter* **2000**, *61*, 7459.
(23) Grunes, L. A. *Phys. Rev. B: Condens. Matter* **1983**, *27*, 2111.
(24) Ankudinov, A. L.; Rehr, J. J.; Bare, S. R. *Chem. Phys. Lett.* **2000**, *316*, 495.
(25) *The Iron Oxides: Structure, Properties, Reactions, Occurrence and Uses*; Cornell, R. M., Schwertmann, U., Eds.; 1996.
(26) Draeger, G.; Frahm, R.; Materlik, G.; Bruemmer, O. *Phys. Status Solidi B* **1988**, *146*, 287.
(27) Finkelstein, K. D.; Shen, Q.; Shastri, S. *Phys. Rev. Lett.* **1992**, *69*, 1612.
(28) Wu, Z.; Xian, D. C.; Natoli, C. R.; Marcelli, A.; Paris, E.; Mottana, A. *Appl. Phys. Lett.* **2001**, *79*, 1918.
(29) Modrow, H.; Bucher, S.; Rehr, J. J.; Ankudinov, A. in press.
(30) Draeger, G.; Czolbe, W.; Leiro, J. A. *Phys. Rev. B: Condens. Matter* **1992**, *45*, 8283.
(31) *Physical Inorganic Chemistry: Coordination Chemistry Approach*; Kettle, S. F. A., Ed.; 1996; p 512.
(32) Bedzyk, M. J. Private communication.
(33) Rajh, T.; Chen, L. X.; Lukas, K.; Liu, T.; Thurnauer, M. C.; Tiede, D. M. submitted for publication, 2002.
(34) Rajh, T.; Poluektov, O.; Dubinski, A. A.; Wiederrecht, G.; Thurnauer, M. C.; Trifunac, A. D. *Chem. Phys. Lett.* **2001**, *344*, 31.
(35) Chen, L. X.; Rajh, T.; Liu, T.; Freeland, J. Unpublished results.